

## Field-effect mobility of amorphous silicon thin-film transistors under strain

H. Gleskova<sup>a,\*</sup>, P.I. Hsu<sup>a</sup>, Z. Xi<sup>b,1</sup>, J.C. Sturm<sup>a</sup>, Z. Suo<sup>b,2</sup>, S. Wagner<sup>a</sup>

<sup>a</sup> Department of Electrical Engineering, Princeton University, Princeton, NJ 08544, USA

<sup>b</sup> Department of Mechanical and Aerospace Engineering, Princeton University, Princeton, NJ 08544, USA

### Abstract

We applied strain ranging from 1% compressive to ~0.3% tensile to a-Si:H TFTs on polyimide foils by bending them inward or outward, or by stretching them in a microstrain tester. We also applied strain to a-Si:H TFTs by deforming a flat substrate into a spherical dome. In each case, compression lowered and tension raised the on-current and hence the electron field-effect mobility. We conclude that compressive strain broadens both the valence and conduction band tails of the a-Si:H channel material, and thus reduces the effective electron mobility. We show that the mobility can be used as an indicator of local mechanical strain.

© 2004 Elsevier B.V. All rights reserved.

PACS: 85.30.Tv; 81.05.Gc; 68.60.Bs

### 1. Introduction

Flexible electronics based on amorphous silicon (a-Si:H) thin-film transistors (TFTs) is a field of rapidly growing interest, to the display industry and for large-area electronics in general. Thus building transistor electronics resistant to mechanical strain has become very important. This need has stimulated research on the interdependence of the electrical and mechanical characteristics of a-Si:H and TFTs made from it. We have systematically studied the electro-mechanical characteristics of a-Si:H TFTs under cylindrical bending and uniaxial stretching [1,2]. In this paper we show that the a-Si:H TFT can be used to evaluate local strain.

The piezoresistive effect, or in other words, the change in the resistance of a material caused by strain, has been reported for many materials. The resistivity depends on strain through either the mobility or the number of the free charge carriers (the band gap of semiconductors

changes with the strain). The piezoresistance of crystalline silicon is highly anisotropic [3]; the effective mass of electrons, and thus the mobility, is determined by the six energy minima of the conduction band [4,5]. Applied uniaxial strain disturbs the cubic symmetry of the crystal. Stretching along a [1 0 0] axis increases the energy of the valleys on that axis and transfers the electrons to the [0 0 1] and [0 1 0] valleys. Since the constant energy surface of each valley is an ellipsoid elongated along the corresponding axis, the electrons in [0 0 1] and [0 1 0] valleys have higher mobility in the [1 0 0] direction, raising the conductivity in that direction. If the strain is small, the change in the electrical conductivity is linearly proportional to the strain.

The change in the resistance (conductance) of a-Si:H as a function of strain has been studied by several authors [6–8], even though the lack of long-range order should attenuate any piezoresistive effect. The results of these measurements have been contradictory, because the piezoresistance is found to depend on the method of preparation and the conductivity type. A detailed study of glow-discharge a-Si:H films [7] revealed that the conductance of undoped and (n<sup>+</sup>) a-Si:H material increases (decreases) with increasing uniaxial tensile (compressive) strain. On the other hand, the conductance of p-type a-Si:H decreases (increases) with increasing uniaxial tensile (compressive) strain. The

\* Corresponding author. Tel.: +1-609 258 4626; fax: +1-609 258 3585.

E-mail address: [gleskova@princeton.edu](mailto:gleskova@princeton.edu) (H. Gleskova).

<sup>1</sup> Present address: Center for Composite Materials, University of Delaware, Newark, DE 19716, USA.

<sup>2</sup> Present address: Division of Engineering and Applied Sciences, Harvard University, Cambridge, MA 02138, USA.

magnitude of the conductance depends on the directions of the applied strain and the current path with respect to each other. The largest change is observed when the strain is parallel to the current path, and the smallest when the strain is perpendicular to the current path. The authors concluded that the application of tensile strain to n- or p-type a-Si:H always shifts the Fermi level towards the conduction band edge, while compressive strain shifts the Fermi level towards the valence band edge. The cause of this Fermi level shift remains to be explained.

The effect of strain on the performance of a-Si:H-based devices has been studied sporadically [9,10]. The field-effect mobility of a-Si:H TFTs under compressive strain was found to decrease [9]. The forward and reverse currents of p–i–n a-Si:H junctions decreased (increased) under tensile (compressive) strain applied parallel to the junction plane [10].

Three regimes can be observed in the electrical/mechanical characteristics of a-Si:H TFTs made on polyimide foil substrates [2]. (1) At low strain, the field-effect mobility changes reversibly. These changes are induced by elastic deformation. (2) At high tensile strain, electrical instabilities appear that are partially reversible, depending on strain–time history. These instabilities arise from the opening and re-closing of cracks in TFT layers under force exerted by the viscoelastic polymer substrate. Such instabilities are not observed in compression. (3) The definitive opening of cracks in TFT layers causes permanent electrical failure. This paper will concentrate on changes in the mobility at low strain.

## 2. Experiments

We fabricated arrays of a-Si:H TFTs on 51  $\mu\text{m}$  thick Kapton E polyimide at the maximum process temperature of 150  $^{\circ}\text{C}$ . First, the polyimide substrate was coated on both sides with a 0.5  $\mu\text{m}$  thick layer of  $\text{SiN}_x$ . The TFTs have the inverted, bottom gate staggered geometry with  $\text{SiN}_x$  back-channel passivation. All TFTs have the following structure:  $\sim 100$  nm thick Ti/Cr layer as gate electrode,  $\sim 360$  nm of gate  $\text{SiN}_x$ ,  $\sim 100$  nm of undoped a-Si:H, 180 nm of passivating  $\text{SiN}_x$ ,  $\sim 50$  nm of ( $n^+$ ) a-Si:H, and  $\sim 100$  nm thick Al for the source–drain contacts. Fabrication details are given elsewhere [11]. The channel length is 40  $\mu\text{m}$  and the channel width 400  $\mu\text{m}$ . After fabrication, the  $\text{SiN}_x$  layer on the back of the substrate was etched away and the transistors were annealed in forming gas. A typical off-current was  $\sim 3 \times 10^{-12}$  A, the on–off current ratio  $> 10^6$ , the threshold voltage  $\sim 3$  V, and the subthreshold slope  $\sim 0.5$  V/decade. The electron mobility, calculated from the transfer characteristic for drain-to-source voltage  $V_{ds} = 0.1$  V, was  $\sim 0.45$   $\text{cm}^2/\text{V s}$ .

We strained the transistors by either bending or stretching. Since the length and width of Kapton substrate are orders of magnitude larger than its thickness, the applied strain is uniaxial. Inward cylindrical bending produces compression, by definition negative, and outward bending tension, positive. The bending direction was parallel or perpendicular to the source–drain current path. The bending radius determined the strain in the TFT and the details of this experiment can be found elsewhere [1]. Additional a-Si:H TFTs were subjected to uniaxial tensile strain in a microstrain tester [2]. Individual TFTs were firmly clamped between two jaws, one stationary and one movable, of the tester. A controlled load was applied to the movable jaw and measured with a load cell. The stretching direction was parallel to the source–drain current path. Transfer characteristics were measured for each radius of curvature (bending) or load (stretching). From each set of transfer characteristics we extracted the off-current, on-current, gate leakage current, mobility  $\mu$ , threshold voltage, and subthreshold slope. Here we will only report the field-effect mobility.

Similar a-Si:H TFTs were fabricated on Kapton foil, which was then permanently deformed to a spherical dome [12]. To perform the deformation, the substrate was clamped by a ring of 6 cm in diameter. Pressurized gas then deformed the material within the clamped ring to a spherical dome of  $\sim 1$  sr ( $66^{\circ}$  field-of-view). During this deformation, the substrate is in tension and undergoes plastic deformation. The devices at the top of the dome are under tensile strain that exceeds 5%. a-Si:H TFTs fracture at  $\sim 0.3\%$  of tensile strain. To avoid fracture, the TFTs are fabricated on rigid islands that are separated from each other by bare plastic substrate. Since the thickness of Kapton substrate is negligible compared to the size and the radius of curvature of the dome, the islands are under biaxial strain. During spherical deformation, the substrate exposed between the islands takes up most of the plastic deformation, leaving the rigid islands crack-free. To increase the maximum size of crack-free islands, they were fabricated on top of mesas made by etching about 10  $\mu\text{m}$  into the polyimide. TFT transfer characteristics were measured before and after deformation.

## 3. Results

The results of the uniaxial cylindrical bending are summarized in Fig. 1. The normalized mobility  $\mu/\mu_0$  is plotted as a function of strain  $\epsilon$ , where  $\mu$  is the field-effect mobility under an imposed strain and  $\mu_0$  is the initial mobility. Each symbol on the graph represents a different TFT. The empty and full symbols correspond to TFT currents parallel and perpendicular to the bending direction, respectively. There is no difference in  $\mu/\mu_0$  with the direction of the strain, except that  $\mu/\mu_0$  is

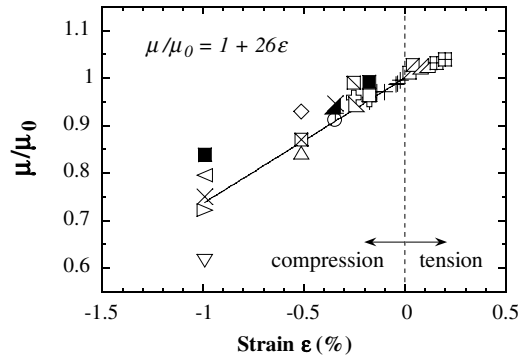


Fig. 1. Normalized electron field-effect mobility plotted as a function of strain. Each symbol represents a different TFT. Empty and full symbols correspond to TFTs with the bending direction parallel and perpendicular to the source–drain current path, respectively. The linear fit is for TFTs with the bending direction parallel to the source–drain current path.

slightly larger in the perpendicular direction. A linear fit to mobilities measured parallel to the bending direction gives:  $\mu/\mu_0 = 1 + 26 \cdot \varepsilon$ .

Fig. 2 shows the mobility in the strain tester for strain along the direction of the source–drain current. The load was increased in small increments up to the breaking point. Initially, the mobility increases as a function of strain and follows the same dependence as observed in the bending experiment. For tensile strains larger than  $\sim 0.2\%$ , the mobility starts to deviate from this behavior. TFT failed at a strain of  $\sim 0.3\%$ .

Polyimide foils with a-Si:H TFT islands sitting on mesas of the same size as the TFT islands were deformed to spherical domes. During maximum deformation the average radial strain was  $\sim 6\%$ . After pressure release, the dome relaxed back to an average radial strain of  $\sim 4\%$ . Fig. 3 shows the normalized mobility  $\mu/\mu_0$  as a function of island size, where  $\mu$  is the field-effect mobility after spherical deformation and  $\mu_0$  is the initial mobility. The mobility decreased after the deformation and de-

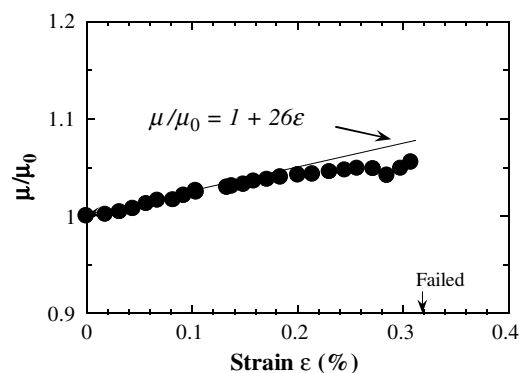


Fig. 2. Field-effect mobility plotted as a function of tensile strain. The TFT was stretched along the direction of the source–drain current path.

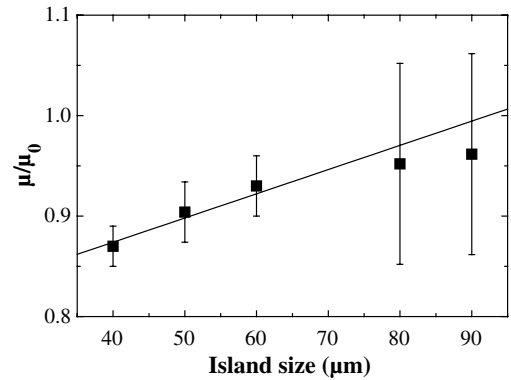


Fig. 3. Field-effect mobility in TFTs on square islands placed on same-size, 10- $\mu\text{m}$  high mesas, as a function of mesa size, with substrate deformed to a spherical cap. The straight line is a least-square fit.

creased more on smaller islands. This indicates that the TFT islands are under compression and the compressive strain is larger in smaller islands. Yet, at the same time, only the islands smaller than  $90 \times 90 \mu\text{m}^2$  remained free of cracks, indicating that at some point the islands had experienced tensile strain that was bigger in bigger islands.

To resolve this puzzle, we used a commercially available finite-element analysis program (ABAQUS) to calculate the strain distribution in the TFT islands on mesas near the top of the dome, where the biaxial strain is uniform [13]. The model structure consisted of a 1  $\mu\text{m}$  thick round islands, 50  $\mu\text{m}$  in diameter, placed on a 10- $\mu\text{m}$  high mesa. We used cylindrical coordinates with the  $z$ -axis perpendicular to the center of the island. Fig. 4 shows the radial strain distribution in the mesa island at maximum deformation ( $\sim 6\%$  strain), and after pressure release ( $\sim 4\%$  strain). The negative radial strain at the center indicates that indeed the islands are in compression, even though the substrate as a whole had been expanded. The calculation also revealed that this compressive strain decreases with increasing island size, in

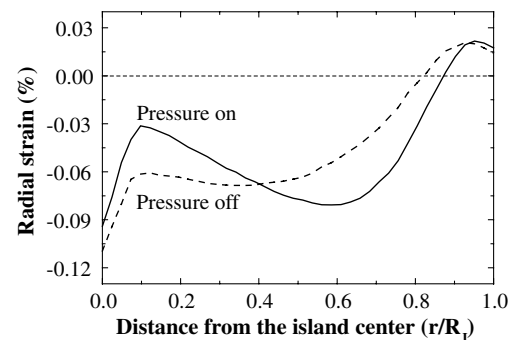


Fig. 4. Finite element analysis of the radial strain in a round amorphous silicon island (thickness = 1  $\mu\text{m}$ , diameter = 50  $\mu\text{m}$ ) on a 10- $\mu\text{m}$  high mesa etched into the 50- $\mu\text{m}$ -thick polyimide substrate, which is deformed to 6% strain (pressure on) and relaxed to 4% strain (pressure off).

agreement with the experimental data. This agreement of model with the experimental mobilities shows that TFTs can be used to evaluate local uniaxial and biaxial strains.

#### 4. Discussion

In contrast to crystalline silicon, the band gap of a-Si:H contains a continuous distribution of localized states: tail states near the band edges, and dangling-bond deep states near midgap. The slopes of the conduction and valence band tails are correlated [14,15] and controlled by the amount of structural and/or thermal disorder [16]. The tail states and deep defects equilibrate, and the position of the Fermi level is determined by the defect distribution.

In a-Si:H TFTs the free electron mobility, which is set by scattering on every silicon atom, is reduced to an effective mobility by frequent trapping in the conduction band tail states of a-Si:H channel material. The bandgap of a-Si:H, which is also affected by disorder [16], was found to decrease with increasing hydrostatic pressure [17]. Uniaxial strain slightly affects the density of dangling bonds, measured by the constant photocurrent method [18]. Compression strongly quenches the photoluminescence in a-Si:H [19], which indicates that raising the pressure suppresses radiative recombination in favor of non-radiative tunneling to defects.

Using the experimental results of Refs. [14–17], we have linked the reduction in the optical band gap of intrinsic a-Si:H under compression to the increased disorder and its effect on the field-effect mobility in a-Si:H. The decrease in the mobility under compression derived from Refs. [14–17] and the mobility drop in our a-Si:H TFTs agree within a factor of two [1].

#### 5. Conclusions

We applied uniaxial strain ranging from 1% compressive to ~0.3% tensile to a-Si:H TFTs on polyimide foil by bending them inward or outward, or by stretching them in a microstrain tester. Compression reduces and tension raises the field-effect mobility. These changes in the mobility qualitatively agree with earlier observations of the piezoresistive effect in a-Si:H. They

appear to be caused by the changes in the slope of the conduction band tail of the a-Si:H channel material.

We also applied biaxial strain to a-Si:H TFTs by deforming a flat substrate into a spherical dome. The changes in the TFT mobility under biaxial strain qualitatively agree with those under uniaxial strain. We show that field-effect mobility can be employed as an indicator of mechanical strain.

#### Acknowledgements

The authors gratefully acknowledge support from DARPA and the New Jersey Commission on Science and Technology.

#### References

- [1] H. Gleskova, S. Wagner, *Appl. Phys. Lett.* 79 (2001) 3347.
- [2] H. Gleskova, S. Wagner, W. Soboyejo, Z. Suo, *J. Appl. Phys.* 92 (2002) 6224.
- [3] C.S. Smith, *Phys. Rev.* 94 (1954) 42.
- [4] R.W. Keyes, in: *Solid State Physics*, vol. 11, Academic Press, New York, 1960, p. 149.
- [5] R.E. Belford, *J. Electron. Mater.* 30 (2001) 807.
- [6] S. Minomura, in: J.I. Pankove (Ed.), *Semiconductors and Semimetals, Part A*, vol. 21, Academic Press, New York, 1984, p. 285, and references within.
- [7] W.E. Spear, M. Heintze, *Philos. Mag.* B 54 (1986) 343.
- [8] W. Fuhs, *Phys. Stat. Sol. (a)* 10 (1972) 201.
- [9] B.L. Jones, *J. Non-Cryst. Solids* 77–78 (1985) 1405.
- [10] M. Utsunomiya, A. Yoshida, *J. Appl. Phys.* 66 (1989) 308.
- [11] H. Gleskova, S. Wagner, V. Gašparik, P. Kováč, *J. Electrochem. Soc.* 148 (2001) G370.
- [12] P.I. Hsu, R. Bhattacharya, H. Gleskova, M. Huang, Z. Xi, Z. Suo, S. Wagner, J.C. Sturm, *Appl. Phys. Lett.* 81 (2002) 1723.
- [13] P.I. Hsu, M. Huang, Z. Xi, S. Wagner, Z. Suo, J.C. Sturm, *J. Appl. Phys.* 95 (2004) 705.
- [14] S. Sherman, S. Wagner, R.A. Gottscho, *Appl. Phys. Lett.* 69 (1996) 3242.
- [15] S. Sherman, P.Y. Lu, R.A. Gottscho, S. Wagner, in: M. Hack, E.A. Schiff, A. Madan, M. Powell, A. Matsuda (Eds.), *Amorphous Silicon Technology – 1995*, vol. 377, Mater. Res. Soc., Pittsburgh, PA, 1995, p. 749.
- [16] G.D. Cody, T. Tiedje, B. Abeles, B. Brooks, Y. Goldstein, *Phys. Rev. Lett.* 47 (1981) 1480.
- [17] B. Welber, M.H. Brodsky, *Phys. Rev. B* 16 (1977) 3660.
- [18] J. Kočka, M. Vaněček, in: A. Madan, M. Thompson, D. Adler, Y. Hamakawa (Eds.), *Amorphous Silicon Semiconductors – Pure and Hydrogenated*, vol. 95, Mater. Res. Soc., Pittsburgh, PA, 1987, p. 83.
- [19] B.A. Weinstein, *Phys. Rev. B* 23 (1981) 787.